BIOMICROFLUIDICS **8**, 052109 (2014)

Migration and vascular lumen formation of endothelial cells in cancer cell spheroids of various sizes

Bishnubrata Patra,[1,2,3] Yu-Sheng Peng,[1,2] Chien-Chung Peng,[3] Wei-Hao Liao,[3] Yu-An Chen,[3,4] Keng-Hui Lin,[5] Yi-Chung Tung,[3,a)] and Chau-Hwang Lee[1,2,3,a)]

[1]*Institute of Biophotonics, National Yang-Ming University, Taipei 11221, Taiwan*
[2]*Biophotonics and Molecular Imaging Research Center (BMIRC), National Yang-Ming University, Taipei 11221, Taiwan*
[3]*Research Center for Applied Sciences, Academia Sinica, Taipei 11529, Taiwan*
[4]*Department of Mechanical Engineering, National Taiwan University, Taipei 10617, Taiwan*
[5]*Institute of Physics, Academia Sinica, Taipei 11529, Taiwan*

(Received 3 June 2014; accepted 1 September 2014; published online 9 September 2014)

We developed a microfluidic device to culture cellular spheroids of controlled sizes and suitable for live cell imaging by selective plane illumination microscopy (SPIM). We cocultured human umbilical vein endothelial cells (HUVECs) within the spheroids formed by hepatocellular carcinoma cells, and studied the distributions of the HUVECs over time. We observed that the migration of HUVECs depended on the size of spheroids. In the spheroids of $\sim$200 μm diameters, HUVECs migrated outwards to the edges within 48 h; while in the spheroids of $\sim$250 μm diameters, there was no outward migration of the HUVECs up to 72 h. In addition, we studied the effects of pro-angiogenic factors, namely, vascular endothelial growth factor (VEGF) and fibroblast growth factor (β-FGF), on the migration of HUVECs in the carcinoma cell spheroid. The outward migration of HUVECs in 200 μm spheroids was hindered by the treatment with VEGF and β-FGF. Moreover, some of the HUVECs formed hollow lumen within 72 h under VEGF and β-FGF treatment. The combination of SPIM and microfluidic devices gives high resolution in both spatial and temporal domains. The observation of HUVECs in spheroids provides us insight on tumor vascularization, an ideal disease model for drug screening and fundamental studies.
© *2014 AIP Publishing LLC*. [http://dx.doi.org/10.1063/1.4895568]

INTRODUCTION

Given the role of vascular network formation in tumor growth and progression, targeting tumor vasculature as a therapeutic method has long been proposed, and the inhibition of endothelial growth factors is one of the practical approaches to restrict tumor angiogenesis.[1] However, previous results with anti-angiogenesis drugs alone have been disappointing despite pre-clinical indications.[2] In a different approach, stabilization and normalization of tumor blood vessels resulted in decreased interstitial fluids, improved tumor oxygenation and enhanced delivery of cytotoxic agents when combined with standard of care.[3,4] As a consequence, useful pre-clinical models are still desirable for the studies on behaviors of endothelial cells under the influences from carcinoma cells.

Multicellular tumor spheroid culture plays more and more important roles in cancer research compared to conventional two-dimensional (2D) cell cultures.[5] A multicellular spheroid establishes gradients in nutrients, metabolites, catabolites, and oxygen in the radial

[a)]Authors to whom correspondence should be addressed. Electronic addresses: tungy@gate.sinica.edu.tw, Tel.: +886-2-2787-3138, and clee@gate.sinica.edu.tw, Tel.: +886-2-2787-3134.

 © 2014 AIP Publishing LLC

direction. Cellular functions and responses in tissues can be mimicked in spheroid cultures, and therefore, cellular spheroids can improve predictive capabilities of assays about drug efficacies.[6,7] Traditional spheroid formation methods such as hanging drops, culture of cells on non-adherent surfaces, spinner flask, or NASA rotary cell culture system usually produce spheroids of random sizes, which are inconvenient for many biomedical applications.[8] For instance, spheroids with various sizes are unable to provide reliable information for drug testing due to the size dependent resistance of tumor spheroids. Many researchers have developed various microfluidic devices for formation and culture of tumor spheroids[9–12] or differentiation of embryoid bodies.[13,14] Some devices were recently used for drug testing on carcinoma spheroids.[15–17] Coculture spheroids for investigating cell–cell interactions in a 3D environment have also been implemented.[18,19] Delicately designed microfluidic devices can provide continuous medium perfusion and better oxygen exchange for spheroid culture.[20,21] Microfluidics is also capable of better flow controls in spatial and temporal domains, which allows reconstituting precise and more *in vivo*-like microenvironments to study cell behaviors. Nonetheless, imaging modality for observing 3D cellular dynamics is also required for the studies and applications of spheroid cultures.

Selective plane illumination microscopy (SPIM) is an optically sectioning microscopy technique for imaging large fluorescence samples such as embryos and cellular spheroids.[6,22] In SPIM, the sample is illuminated with a sheet of light that propagates perpendicularly to the direction of observation. Therefore, a fluorescence image of a finite depth, called sectioned image, can be formed without lateral scanning. A stack of sectioned images acquired as the sample is moved along the direction of observation can be used to form a three dimensional (3D) view of a sample. Owing to the side-wise illumination and wide-field detection, SPIM offers lower photobleaching and phototoxicity compared to confocal microscopy, beneficial for time-lapse 3D imaging of biological samples larger than 100 μm in thickness.[23] For example, in embryos of zebrafish, the imaging of SPIM resulted in normal bone growth; while the observation with confocal microscopy caused aberrant bone growth under equivalent exposure conditions.[24] Although confocal microscopy provides better spatial resolution than usual SPIM, the spatial resolution of SPIM can be further improved by employing proper image deconvolution methods, such that a single cell can be identified in a sample larger than 100 μm.[25] With these unique features, SPIM has been applied to image live cell proliferation processes in cellular spheroids.[23,26,27] However, most of microfluidics devices are not compatible with light sheet microscopy because of the geometries of the culture chambers or the arrangement of the flow channels.

A simple microfluidic device compatible with SPIM can facilitate the time-lapse observation on cellular dynamics or formation of multicellular structures in spheroid cultures. In this work, we used a simple microfluidic device made of polydimethylsiloxane (PDMS) to form cocultured spheroids of hepatocellular carcinoma cells (HepG2) and human umbilical vein endothelial cells (HUVECs).[28] In this device, the cubical spheroid culture chambers made it easy to accommodate the illumination light sheet of SPIM as well as to capture the fluorescence images of the cells. We could also control the spheroid size using various sizes of cubical cavities in a same device. Using a single-beam SPIM setup, we studied the behavior of HUVECs in a particular spheroid up to 72 h. We found that the migration of HUVECs was related to the size of the tumor cell spheroids. With this platform, we also evaluated the effects of growth factors, including vascular endothelial growth factor (VEGF), and fibroblast growth factor (β-FGF) on the HUVECs inside the tumor spheroids. Under the treatment of VEGF and β-FGF, the HUVECs tended to stay inside the tumor cell spheroids, and some of the HUVECs formed lumen-like structures.

MATERIALS AND METHODS

Design and fabrication of the spheroid culture device

The culture device for cellular spheroids was constructed using two PDMS layers: The bottom layer contained the culture chambers while the top layer held one channel covering the culture chambers, as shown in Fig. 1. We arranged the culture chambers such that the light sheet

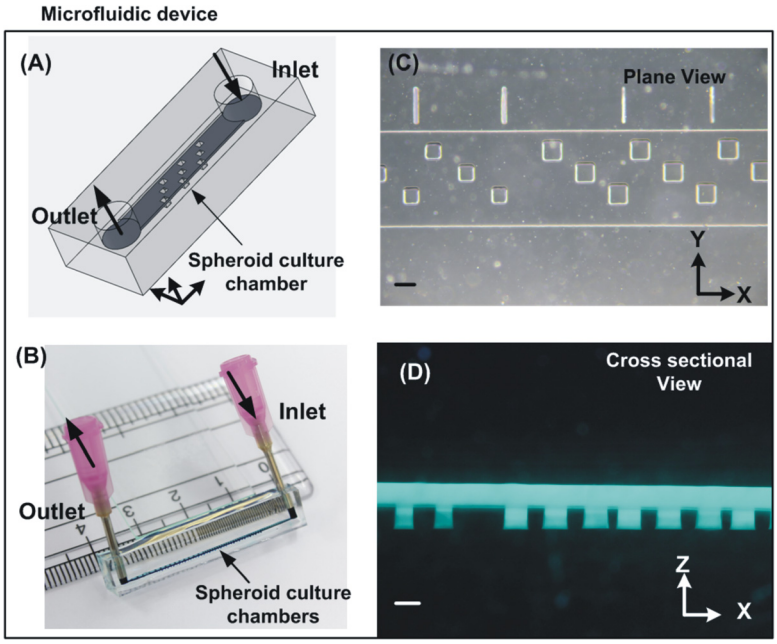

FIG. 1. (A) Illustrations of the microfluidic device for spheroid formation, culture, and imaging by SPIM. The spheroid culture chambers are organized in a way such that only a single spheroid is illuminated at a time. (B) Photo of the fabricated microfluidic device. The scale on the ruler is cm. (C) and (D) Microscopic plane and cross-sectional view of the device filled with fluorescein. Scale bars in (C) and (D), 250 μm.

of SPIM illuminated only one chamber at a time [Fig. 1(A)]. This device was fabricated using the well-developed soft lithography replica molding process. In brief, a silicon wafer with positive relief features was exploited as a mold. The mold was fabricated using a negative tone photoresist (SU-8 2050, Micro Chem Co., Newton, MA) patterned by photolithography. The fabricated mold was then silanized with 1H,1H,2H,2H-perfluorooctyltrichlorosilane (78560–45-9, AlfaAesar, Ward Hill, MA) in a desiccator for more than 30 min at room temperature to prevent undesired bonding of PDMS to the mold. PDMS prepolymer (Sylgard 184, Dow Corning Co., Midland, MI) with a 1:10 (v/v) curing agent to base ratio was poured on the mold and cured at 60 °C for more than 4 h. After curing, we made the interconnection holes by using a biopsy punch with a diameter of 1.5 mm at the top layer. The bottom layer was aligned and irreversibly bonded with the top layer by using oxygen plasma surface treatment at 90 W for 40 s. The PDMS device was then cured in a 60 °C oven for more than 2 h to promote the bonding and to assure full curing of the PDMS for better cellular compatibility. The bottom layer of the device ($4 \times 0.75 \times 0.75$ cm) was made as thin as possible to be compatible with the observation of SPIM [Fig. 1(B)]. A thin glass slide was attached to the device to make its shape more stable during experimental operations. In this device, we prepared cubical spheroid culture cavities with areas of $200 \times 200\ \mu m^2$ and $250 \times 250\ \mu m^2$ [Fig. 1(C)]. In order to minimize the light scattering, a thin layer of the PDMS precursor was applied on the device sidewall and then cured at 60 °C. We kept the surface face up and leveled for more than 2 h to smoothen the introduction surface of the light sheet. Figure 1(D) shows the cross sectional view of the device filled with fluorescein. The depth and height of the cavities and top channel were both 250 μm.

Experimental setup

Figure 2 shows the setup of our experiments. We used an inverted microscope (TS-100F, Nikon, Kanagawa, Japan) as the main frame of our SPIM system. The light source was a supercontinuum laser with visible power (wavelength 450–750 nm) larger than 300 mW (Fianium, Southampton, UK). Neutral density filters of various transmissions were used to control the laser

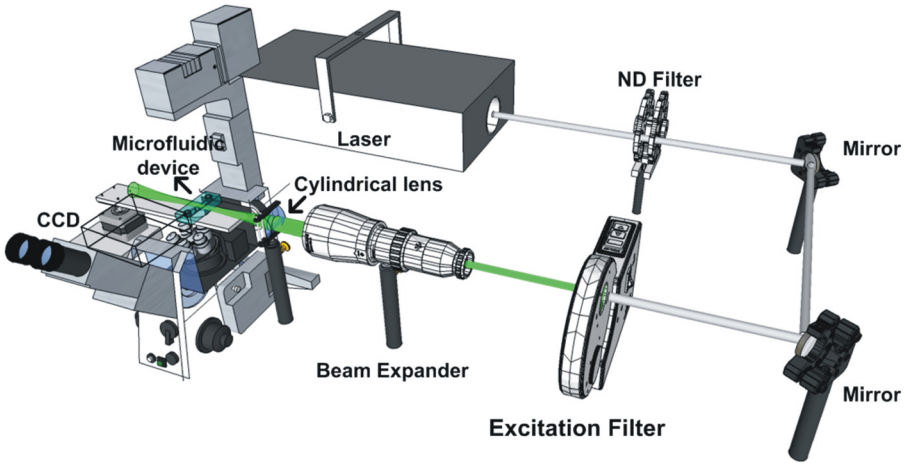

FIG. 2. Schematic diagram of the SPIM setup.

power. A motorized filter wheel (FW102C, Thorlabs, Newton, NJ) was used for selecting the excitation filters. A filter centered at 470 nm with a 40 nm full width at half maximum (FWHM) of the pass band was used for the excitation of Cell Tracker Green, and a filter centered at 545 nm, with a 30 nm FWHM of the pass band was for DsRed. A beam expander was used to achieve the required beam diameter at the cylindrical lens. We used a cylindrical lens with a 5 cm focal length to generate the illumination light sheet for SPIM. At the focal point of the cylindrical lens, the width of the light sheet was estimated to be 300 μm and the thickness was 9.2 μm and 10 μm for the 470 nm and 545 nm excitation beam, respectively. We used a $20\times$/0.50 NA (Leica Microsystems, Wetzlar, Germany) water-immersion objective or a $40\times$/0.60 NA (NIKON, Kanagawa, Japan) dry objective to collect the fluorescence signal. The fluorescence signal was collected by an emission filter centered at 535 nm, with a 50 nm FWHM of the pass band for Cell Tracker Green and an emission filter centered at 600 nm, 50 nm FWHM of the pass band for DsRed. A motorized Z-axis stage with 2 μm positioning accuracy (TSDM(GS)60–10ZF, Sigma-koki, Tokyo, Japan) mounted on a manual X-Y stage was used to hold the microfluidic device. The motion of the Z-axis stage and the image acquisition procedures were controlled by a LabVIEW program. A 14-bit CCD camera (SPOT RT3, Diagnostic Instruments, Sterling Heights, MI) was used to capture the images. The bright-field images were taken with the same microscope. The 3D fluorescence images shown in Figs. 3–5 were constructed using Imaris 7.2.3 (Bitplane, Zurich, Switzerland) after deconvolution with Huygens Essential (Scientific Volume Imaging b.v., Alexanderlaan, The Netherlands).

Cell culture

Human hepatocellular carcinoma cell (HepG2, 60025, Bioresource Collection and Research Center, Hsinchu, Taiwan) was maintained at 37 °C in a humidified incubator with 5% CO_2. The culture medium was composed of Dulbecco's Modified Eagle Medium (DMEM) (Gibco 10566, Invitrogen Co., Carlsbad, CA) with 10% (v/v) fetal bovine serum (Gibco 10082, Invitrogen), 1% (v/v) antibiotic-antimitotic (Gibco 15240, Invitrogen), 1% (v/v) sodium pyruvate (Gibco 11360, Invitrogen), and 1% (v/v) non-essential amino acids (Gibco 11140, Invitrogen). The stocks were maintained in a T25 cell culture flask (Nunc 156367, Thermo Scientific Inc., Rochester, NY), and passaged by dissociation with 0.25% trypsin-EDTA (Gibco 25200, Invitrogen). Cell suspensions for the experiments were made by centrifugation of dissociated cells at 1000 rpm for 5 min at room temperature. Human umbilical vein endothelial cells (HUVEC, C2519A, Lonza, Basel, Switzerland) were cultured with EGM™–2 BulletKit™ Medium (CC-3162, Lonza) in a 37 °C humidified incubator with 5% CO_2 and passaged by dissociation with 0.25% trypsin-EDTA. For all the experiments, the HUVECs were used within 4 to 10 passage numbers.

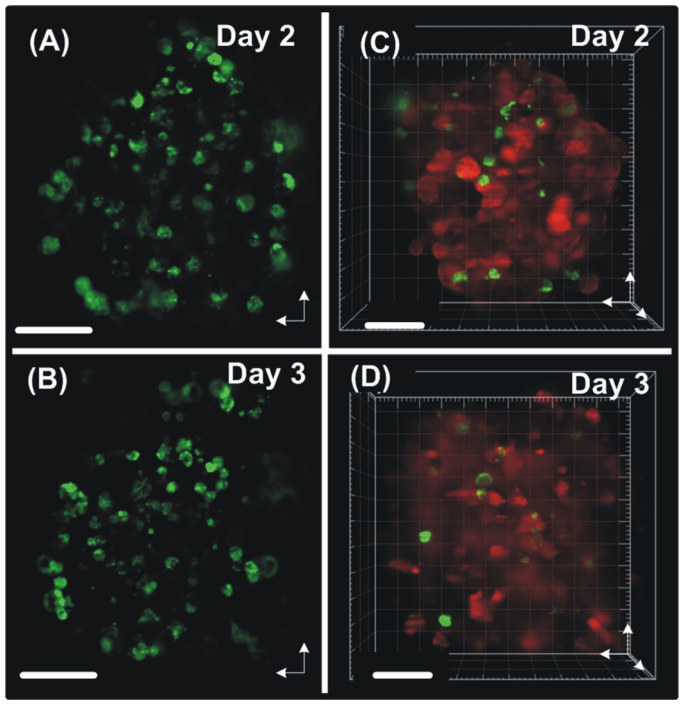

FIG. 3. HepG2 cell (red) and HUVEC (green) coculture spheroid observed by SPIM (after deconvolution) with a 20× water-immersion objective. (A) and (B) single slice 2D images of the HUVECs inside a spheroid at day 2 and day 3. (C) and (D) 3D rendering view of the coculture spheroid at day 2 and day 3. Scale bar—80 μm.

Cell spheroid formation and culture

Before the experiments, the device was oxidized in oxygen plasmas for 40 s to make the PDMS surface hydrophilic. Afterwards, 1% (v/v) Synperonic® F-108 (07579, Fluka, SIGMA-ALDRICH, Co., St Louis, MO, USA) was introduced into the channel and incubated overnight to make the device resistant to cell adhesion. Prior to cell loading, the device was sterilized under ultraviolet light for 1 h. Excess Synperonic® F-108 was washed out with the HepG2 and HUVEC culture media mixed with a 1:1 volume ratio. For the formation and culture of coculture spheroids, the top channel with length, width, and height of $38 \times 1.2 \times 0.25\,\text{mm}^3$ and the culture chambers with length, width, and depth of $200 \times 200 \times 250\,\mu\text{m}^3$ (small chamber) and $250 \times 250 \times 250\,\mu\text{m}^3$ (large chamber) were used (total 54 chambers). A 5 μl cell suspension with a ratio HepG2:HUVEC (50 μM Cell Tracker Green in 2 ml DMEM, incubated by 20 min)-$=$5:1 with a density of 10^7 cells/ml was introduced from the top channel inlet at a flow rate-$\sim$1.0 μl/min. The device was kept in a humidified incubator with 5% CO_2 at 37 °C. The cells settled in the culture chambers gradually because of the gravity. Owing to the strong cell–cell interaction and non-adhesive surface of the device, the cells aggregated with each other within 24 h. The culture medium was refreshed after 12 h using a normal pipette with a flow rate $\sim$20 μl/min. For the drug-treatment experiments, we added 1 μl, 10 μg/ml VEGF (100–20, Peprotech, Rocky Hill, NJ) and 1 μl, 10 μg/ml β-FGF (100–18B, Peprotech) into 100 μl HUVEC culture medium, and then injected the solution into the spheroid culture device.

Areal distribution of HUVEC in percentage

In order to study the HUVEC migration, a MATLAB program was used to analyze 2D image slices at various time points, as illustrated in Fig. S1 in the supplementary material.[29] The area occupied by HUVECs in an annular ring of middle radius r with a width of 10 μm was normalized by the area of this annular ring. We named this value as the "percentage of HUVEC occupied area in the annular ring of radius r." Then a histogram of "percentage of

HUVEC occupied area in a particular annular ring" was drawn with normalized ring radius (r/R) by the MATLAB program, where R is the spheroid radius.

RESULTS

Resolution of SPIM in the spheroid culture device

The cubical cavities of our spheroid culture device caused little influence in the illumination light path of the SPIM. The smooth device side walls also helped to minimize the scattering. To characterize the resolution of our SPIM setup, we used 200 nm fluorescent beads in agarose and took Z-stacks of 2D images with an excitation filter at 470 nm and an emission filter at 535 nm. We reconstructed a 3D image from these 2D images and measured the point spread function (PSF) along the X, Y, and Z axes using the MetroloJ plug-in in the Fiji image processing package.[30] By using the $20\times/0.50$ NA water-immersion objective to capture the images, the measured FWHM of the PSF was 0.67 μm and 0.63 μm in the X and Y axis, respectively. The average width of the Z-axis PSF was about 11 μm with careful alignment.

SPIM images of cellular spheroids

In Fig. 3, we show a coculture spheroid (diameter $\sim$240 μm) of HepG2 (red) and HUVEC (green) imaged at day 2 and day 3 by using the $20\times/0.50$ NA water-immersion objective. Figures 3(A) and 3(B) show single 2D images of the HUVECs inside the spheroid. The HUVECs are distributed randomly in the spheroid. Figures 3(C) and 3(D) show the reconstructed 3D images of the coculture cell spheroid. The results suggest that the integrity of the spheroid should be intact during the SPIM imaging up to day 3.

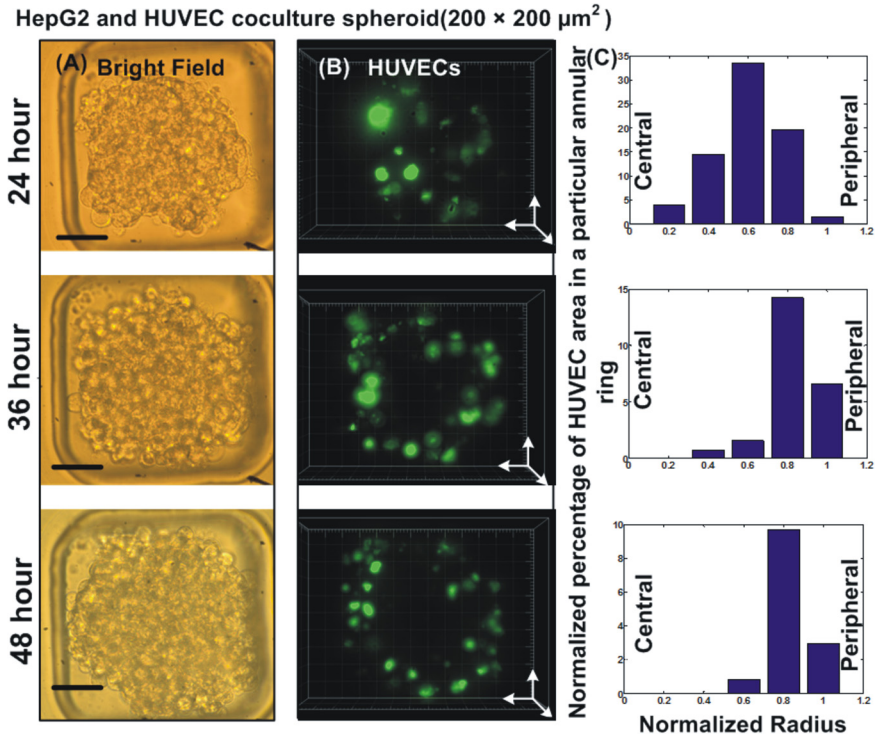

FIG. 4. (A) Time lapse bright-field images of a coculture spheroid in a $200\times200\times250\,\mu m^3$ cubical culture chamber. Scale bar—50 μm. (B) 3D SPIM images of HUVECs cultured inside the HepG2 cell spheroid shown in (A). The HUVECs migrated outside the spheroid with time. (C) Normalized HUVEC area distributions of two-dimensional single image slices of a spheroid cultured in a $200\times200\times250\,\mu m^3$ cubical culture chamber at different time points. The areal distribution confirms the outward migration of the HUVECs.

Migration of HUVECs in spheroids of different sizes

We studied the growth of a particular spheroid up to 48 h by using bright-field images captured with the $40\times/0.60$ NA dry objective. The cellular spheroid was cultured in a $200\times200\,\mu m^2$ cubical chamber. The bright-field images [Fig. 4(A)] confirm the integrity and healthy nature of the spheroid in the microfluidic device after the consecutive imaging using SPIM at 24, 36, and 48 h. Figure 4(B) shows the 3D image of HUVECs cultured in the $200\times200\,\mu m^2$ chamber after 24, 36, and 48 h. The 3D pictures show that at first the HUVECs were randomly distributed in the spheroid. At the 36th h, the HUVECs were migrating outward the spheroid. At 48th h, the outward migration persisted. We compare the normalized percentage of HUVEC area distributions of a single slice at the middle of the spheroid and show the pattern with time in Fig. 4(C). In the smaller spheroid, the HUVECs showed an outward migration tendency. In comparison, Fig. 5(A) shows the bright-field image of the spheroid cultured in the $250\times250\,\mu m^2$ chamber up to 72 h. Figure 5 (B) shows the 3D images of HUVECs inside the spheroid at 24, 48, and 72 h. Figure 5(C) shows the normalized percentage of HUVEC area distributions. We did not see the HUVEC migration in this larger cavity. This phenomenon was repeatedly observed in three experiments.

Formation of a lumen-like structure by the HUVEC

In another set of experiments, we studied the effect of pro-angiogenic factors VEGF and β-FGF on the HUVECs[31] inside the HepG2 spheroid. We added 1 μl VEGF (10 μg/ml) and 1 μl β-FGF (10 μg/ml) into 100 μl HUVEC culture medium, and then injected the solution into the culture device after the first SPIM imaging at 24th h. The total volume of the culture medium inside the device was about 1 ml in static culture condition. Figures 6(A), 6(B), and 6(C), surface plot images generated by Imaris, show the results after 24, 48, and 72 h for a spheroid in a $200\times200\,\mu m^2$ cubical chamber. At 72nd h, we could see a lumen-like structure formed by

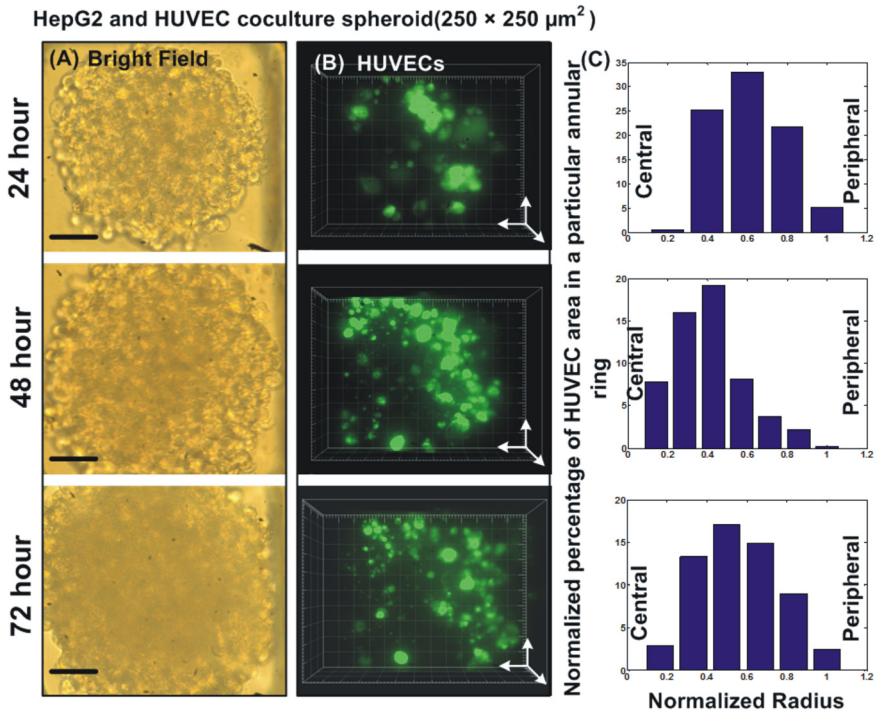

FIG. 5. (A) Time lapse bright-field images of a coculture spheroid in a $250\times250\times250\,\mu m^3$ chamber. Scale bar—50 μm. (B) 3D SPIM images of HUVECs cultured inside the HepG2 cell spheroid shown in (A). The HUVECs did not migrate out. (C) Normalized areal distribution of the HUVECs in a $250\times250\times250\,\mu m^3$ cubical cell culture chamber did not show the outward migration.

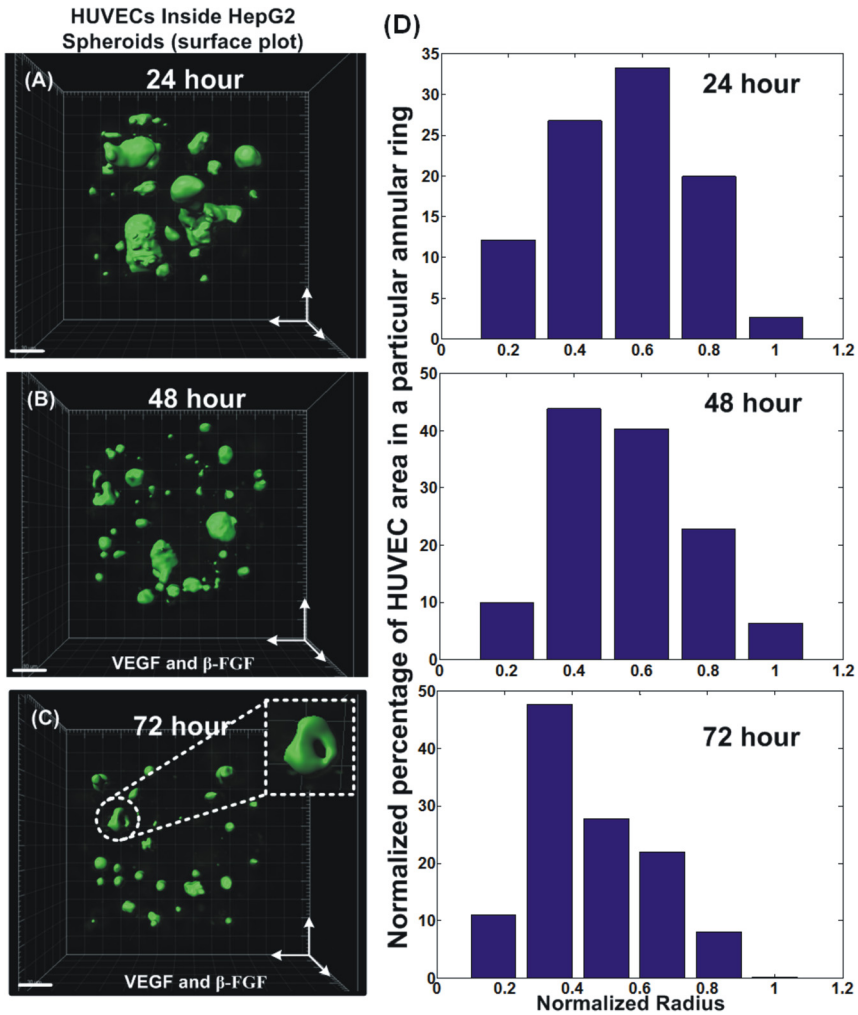

FIG. 6. Surface plot images. (A) HUVECs inside the HepG2 spheroids at 24 h cultured in a $200 \times 200 \times 250\,\mu m^3$ cubical cell culture chamber. (B) and (C) HUVECs inside the same spheroid with the treatment of VEGF and β-FGF at 48 and 72 h. Some HUVECs form circular-cross sectional lumen structure after 48 h of treatment. Scale bar, $30\,\mu m$. (D) Normalized areal distribution of the HUVECs did not show the outward migration.

the HUVEC inside the spheroid. We also calculated the normalized percentage of HUVEC area distributions and show them in Fig. 6(D). Under the treatment of VEGF and β-FGF, we did not find the outward migration of the HUVECs even in the smaller spheroid.

DISCUSSION

We fabricated a multicellular spheroid culture device with cubical culture chambers. The sizes of cellular spheroids were controlled by the dimensions of the cubical chambers. The straight walls of these chambers were well compatible with the SPIM technique that gives much deeper insight to the *in vitro* spheroid culture models. We only used a static culture condition with the device in this present work to avoid unexpected fluid force caused cellular responses such as epithelial–mesenchymal transition mentioned in 3D ovarian cancer nodules.[32]

Studies on endothelial cells that form perfusable microvascular networks and endothelial sprouting have been demonstrated in 3D gel structures.[33,34] In our experiments, we observed a particular cellular spheroid for three days, owing to both the stable microenvironments in the culture device and the low phototoxicity of SPIM.[6,23,35] The images in Fig. 3 demonstrate that the HUVECs inside the HepG2 spheroids can be clearly observed by our SPIM system. With a

$40\times/0.60$ NA objective, the 3D resolution is sufficiently high for identifying individual cells. We also employed bright-field imaging to monitor the growth of coculture spheroids in the device.

Timmins *et al.* had reported that HUVECs were predominantly localized to the outer regions in coculture spheroids with colorectal carcinoma cells.[36] But the authors did not conduct time-lapse sectioning imaging for analyzing the 3D migration of the HUVECs in the spheroid. In the present work, we employed the SPIM to observe the outward migration of HUVECs cocultured in the carcinoma cellular spheroid of a diameter $\sim 200\,\mu$m. However, for $\sim 250\ \mu$m cellular spheroids, the HUVECs exhibited the tendency to stay inside the spheroid and kept proliferating. The up-regulation of several pro-angiogenic factors in endothelial cells has been known to occur in response to the hypoxic environments.[37] Although we tried to use the fluorescently labelled antibody of hypoxia-inducible factor 1α (HIF-1α) to indicate the levels of hypoxia in spheroids, the antibody could only be tagged onto the cells at the periphery of a spheroid. The fluorescent reporters might not be a suitable method to indicate the levels of hypoxia in spheroids. Recently, Grimes *et al.* used positron emission tomography to estimate the oxygen levels in multicellular spheroids.[38] They showed that the spherical oxygen diffusion limit $r_l = 232 \pm 22\,\mu$m for multicellular spheroids. Because the radii of our spheroids were nearly half of the r_l, we postulate that the oxygen levels inside the $250\,\mu$m spheroids were lower than those in the $200\,\mu$m spheroids. Therefore, the intracellular VEGF expression of the HUVECs should be increased.[36] The higher hypoxia state could be the reason for the HUVECs to stay at the center of a large spheroid.

We also studied the effects of exogenous VEGF and β-FGF on the migration of HUVECs inside the coculture spheroid. These pro-angiogenic factors hindered the outward migration of HUVECs even in smaller spheroids. In some cases, we could see that HUVECs formed a vascular lumen-like structure inside the spheroid under the treatment of VEGF and β-FGF. This result demonstrated that our microfluidic platform incorporated with SPIM can help to evaluate the effects of various factors that bring positive or negative influences on vascular lumen formation in tumor spheroid models. However, at present, we have not seen vascular tree formation in our spheroid culture device. More experimental works are necessary to find out the optimized culture condition for vascular tree formation in cellular spheroids.

CONCLUSION

In the present work, we report a microfluidic device for tumor spheroid formation and coculture with endothelial cells. The formation of coculture spheroids was achieved with simple cubical chambers. Because of the straight and transparent chamber walls, this device was compatible to optical imaging techniques. We used a single beam SPIM setup with two-color excitations to study the cellular behaviors in the coculture spheroids. The spheroids formed by hepatocellular carcinoma cells and HUVECs could be cultured for up to three days in this device. The low phototoxicity of the SPIM technique facilitated long-term time-lapse observations on the coculture spheroids. We found outward migration of HUVECs in the carcinoma cell spheroid cultured in a $200\times200\,\mu\text{m}^2$ chamber. In contrast, this kind of outward migration was not observed in spheroids cultured in $250\times250\,\mu\text{m}^2$ chambers. This result could be explained with the mechanism of intracellular VEGF up-regulation by the hypoxia condition in a large spheroid. We also found that pro-angiogenic factors impeded the outward migration of HUVECs and induced the formation of lumen-like structures.

Because of the simplicity in fabrication and operation, the microfluidic device and SPIM platform developed in this work are useful for the studies on the effects of new drugs or drug combinations for both pro-angiogenic and anti-angiogenic therapies. The low phototoxicity of SPIM enables long-term observations of tumor and vessel development without interrupting the multicellular culture. This platform will also benefit studies on other physiological phenomena related to spheroid formation and 3D cell–cell interactions in microenvironment established by various types of cells, such as differentiation of stem cells in embryonic spheroids or neuron cell division and migration in neurospheres.

ACKNOWLEDGMENTS

This work was financially supported by the Ministry of Science and Technology of Taiwan (Contract Nos. NSC 100-2112-M-001-022-MY3 and NSC 101-2628-E-001-002-MY3), and the National Health Research Institutes (Contract No. NHRI EX103-10021EC).

[1]J. Flockman, New Eng. J. Med. **285**, 1182 (1971).
[2]Y. Sato, Int. J. Clin. Oncol. **8**, 200 (2003).
[3]R. K. Jain, Science **307**, 58 (2005).
[4]D. Chakroborty, C. Sarkar, H. Yu, J. Wang, Z. Liu, P. S. Dasgupta, and S. Basu, Proc. Natl. Acad. Sci. U.S.A. **108**, 20730 (2011).
[5]R. Sutherland, Science **240**, 177 (1988).
[6]F. Pampaloni, E. G. Reynaud, and E. H. K. Stelzer, Nat. Rev. Mol. Cell Biol. **8**, 839 (2007).
[7]Y.-C. Tung, A. Y. Hsaio, S. G. Allen, Y. Torosawa, M. Ho, and S. Takayama, Analyst **136**, 473 (2011).
[8]J. Friedrich, R. Ebner, and L. A. Kunz-Schughart, Int. J. Radiat. Biol. **83**, 849 (2007).
[9]S. Agastin, U.-B. T. Giang, Y. Geng, L. A. DeLouise, and M. R. King, Biomicrofluidics **5**, 024110 (2011).
[10]J. Fukuda and K. Nakazawa, Biomicrofluidics **5**, 022205 (2011).
[11]H.-J. Jin, Y.-H. Cho, J.-M. Gu, J. Kim, and Y.-S. Oh, Lab Chip **11**, 115 (2011).
[12]K. Lee, C. Kim, J. Young Yang, H. Lee, B. Ahn, L. Xu, J. Yoon Kang, and K. W. Oh, Biomicrofluidics **6**, 014114 (2012).
[13]G. S. Jeong, Y. Jun, J. H. Song, S. H. Shin, and S.-H. Lee, Lab Chip **12**, 159 (2012).
[14]E. Kang, Y. Y. Choi, Y. Jun, B. G. Chung, and S.-H. Lee, Lab Chip **10**, 2651 (2010).
[15]K. Ziółkowska, R. Kwapiszewski, and Z. Brzózka, New J. Chem. **35**, 979 (2011).
[16]K. Ziółkowska, A. Stelmachowska, R. Kwapiszewski, M. Chudy, A. Dybko, and Z. Brzózka, Biosens. Bioelectron. **40**, 68 (2013).
[17]K. Kwapiszewska, A. Michalczuk, M. Rybka, R. Kwapiszewski, and Z. Brzózka, Lab Chip **14**, 2096 (2014).
[18]A. Y. Hsiao, Y. Torisawa, Y.-C. Tung, S. Sud, R. Taichman, K. J. Pienta, and S. Takayama, Biomaterials **30**, 3020 (2009).
[19]T. Okuyama, H. Yamazoe, N. Mochizuki, A. Khademhosseini, H. Suzuki, and J. Fukuda, J. Biosci. Bioeng. **110**, 572 (2010).
[20]T. Kim and Y.-H. Cho, Lab Chip **11**, 1825 (2011).
[21]T. Anada, J. Fukuda, Y. Sai, and O. Suzuki, Biomaterials **33**, 8430 (2012).
[22]J. Huisken, J. Swoger, F. D. Bene, J. Wittbrodt, and E. H. K. Stelzer, Science **305**, 1007 (2004).
[23]F. Pampaloni, N. Ansari, and E. H. K. Stelzer, Cell Tissue Res. **352**, 161 (2013).
[24]M. Jemielita, M. J. Taormina, A. DeLaurier, C. B. Kimmel, and R. Parthasarathy, J. Biophotonics **6**, 920 (2013).
[25]P. J. Verveer, J. Swoger, F. Pampaloni, K. Greger, M. Marcello, and E. H. K. Stelzer, Nat. Methods **4**, 311 (2007).
[26]C. Lorenzo, C. Frongia, R. Jorand, J. Fehrenbach, P. Weiss, A. Maandhui, G. Gay, B. Ducommun, and V. Lobjois, Cell Division **6**, 22 (2011).
[27]T. Bruns, S. Schickinger, R. Wittig, and H. Schneckenburger, J. Biomed. Opt. **17**, 101518 (2012).
[28]B. Patra, Y.-H. Chen, C.-C. Peng, C.-H. Lee, and Y.-C. Tung, Biomicrofluidics **7**, 054114 (2013).
[29]See supplementary material at http://dx.doi.org/10.1063/1.4895568 for the illustration of the analysis for the percentage of HUVEC occupied area.
[30]R. W. Cole, T. Jinadasa, and C. M. Brown, Nat. Protoc. **6**, 1929 (2011).
[31]F. Shojaei, Cancer Lett. **320**, 130 (2012).
[32]I. Rizvi, U. A. Gurkan, S. Tasoglu, N. Alagic, J. P. Celli, L. B. Menash, Z. Mai, U. Demiric, and T. Hasan, Proc. Natl. Acad. Sci. U.S.A. **110**, E1974 (2013).
[33]S. Kim, H. Lee, M. Chung, and N. L. Jeon, Lab Chip **13**, 1489 (2013).
[34]J. W. Song and L. L. Munn, Proc. Natl. Acad. Sci. U.S.A. **108**, 15342 (2011).
[35]P. J. Keller, F. Pampaloni, and E. H. K. Stelzer, Curr. Opin. Cell Biol. **18**, 117 (2006).
[36]N. Timmins, S. Dietmair, and L. Nielsen, Angiogenesis **7**, 97 (2004).
[37]Y. Liu, S. R. Cox, T. Morita, and S. Kourembanas, Circ. Res. **77**, 638 (1995).
[38]D. R. Grimes, C. Kelly, K. Bloch, and M. Partridge, J. R. Soc. Interface **11**, 20131124 (2014).